Accepted Manuscript

Point collocation scheme in silencers with temperature gradient and mean flow

F.D. Denia, E.M. Sánchez-Orgaz, Luis Baeza, R. Kirby

PII: S0377-0427(15)00068-0
DOI: http://dx.doi.org/10.1016/j.cam.2015.02.007
Reference: CAM 10003

To appear in: *Journal of Computational and Applied Mathematics*

Received date: 15 October 2014
Revised date: 14 January 2015

Please cite this article as: F.D. Denia, E.M. Sánchez-Orgaz, L. Baeza, R. Kirby, Point collocation scheme in silencers with temperature gradient and mean flow, *Journal of Computational and Applied Mathematics* (2015), http://dx.doi.org/10.1016/j.cam.2015.02.007

This is a PDF file of an unedited manuscript that has been accepted for publication. As a service to our customers we are providing this early version of the manuscript. The manuscript will undergo copyediting, typesetting, and review of the resulting proof before it is published in its final form. Please note that during the production process errors may be discovered which could affect the content, and all legal disclaimers that apply to the journal pertain.

ACCEPTED MANUSCRIPT

HIGHLIGHTS

Sound attenuation in perforated dissipative silencers including temperature gradients and mean flow is computed.

A two-dimensional finite element eigenvalue problem is solved for a silencer cross section with transversal thermal variations.

A point collocation scheme is presented to match the acoustic pressure and axial velocity at the silencer geometrical discontinuities.

A significant reduction in the computational requirements is obtained compared to a full three-dimensional finite element approach.

ACCEPTED MANUSCRIPT

Click here to view linked References

ACCEPTED MANUSCRIPT

Point collocation scheme in silencers with temperature gradient and mean flow

F. D. Denia[a,*], *E. M. Sánchez-Orgaz*[a], *Luis Baeza*[a]

[a]*Centro de Investigación de Tecnología de Vehículos, Universitat Politècnica de València, Camino de Vera s/n, 46022 Valencia, Spain*

[*]*fdenia@mcm.upv.es*

R. Kirby[b]

[b]*College of Engineering, Design and Physical Science, Mechanical Engineering, Brunel University, Uxbridge, Middlesex UB8 3PH, UK*

Abstract

This work presents a mathematical approach based on the point collocation technique to compute the transmission loss of perforated dissipative silencers with transversal temperature gradients and mean flow. Three-dimensional wave propagation is considered in silencer geometries with arbitrary, but axially uniform, cross section. To reduce the computational requirements of a full multidimensional finite element calculation, a method is developed combining axial and transversal solutions of the wave equation. First, the finite element method is employed in a two-dimensional problem to extract the eigenvalues and associated eigenvectors for the silencer cross section. Mean flow as well as transversal temperature gradients and the corresponding thermal-induced material heterogeneities are included in the model. In addition, an axially uniform temperature field is taken into account, its value being the inlet/outlet average. A point collocation technique is then used to match the acoustic fields (pressure and axial acoustic velocity) at the geometric discontinuities between the silencer chamber and the inlet and outlet pipes. Transmission loss predictions are compared favorably with a general three-dimensional finite element approach, offering a reduction in the computational effort.

Keywords: Dissipative Silencer; Temperature Gradient; Mean Flow; Point Collocation.

ACCEPTED MANUSCRIPT

ACCEPTED MANUSCRIPT

1. Introduction

Dissipative silencers are widely used in automotive applications due to their acoustic efficiency in the mid and high frequency range. A review of the bibliography published during the last years shows the rise of multidimensional techniques [1-9] to characterize the acoustic behavior of silencers in comparison with one-dimensional techniques, due to their higher accuracy in the silencer operating frequency range.

Among the multidimensional techniques, the finite element method (FEM) presents versatility when the silencer has a complex geometry [4, 5] or when more realistic operating conditions are considered, such as the presence of mean flow [2], heterogeneous properties of the dissipative material [10, 11] and temperature variations [12]. The presence of high temperature and thermal gradients in dissipative silencers modifies their acoustic attenuation performance and the difficulties associated with experimental measurements at high temperatures make it necessary to find computational approaches useful to evaluate the acoustic behavior of the silencer. These numerical techniques have, however, the disadvantage of being computationally expensive when a high number of degrees of freedom is considered. In order to avoid this problem in silencers with arbitrary (but axially uniform) cross section, Kirby [4, 7] obtained the axial wavenumbers (eigenvalues) and pressure modes (eigenvectors) associated with the silencer cross section using a two-dimensional FE model. This transversal eigensolution was then combined with the point collocation technique [4] and, in a later work, with the mode-matching method [6, 7], to obtain the wave amplitudes corresponding to the sound propagation within the different silencer regions. To match the transversal solution with the axially propagating waves, the point collocation technique takes into account the compatibility conditions of the pressure and axial acoustic velocity at the silencer geometric discontinuities. Although this approach delivers a considerable reduction in the computational effort compared to the full three-dimensional FEM, attention has to be paid to some numerical issues, such as those found in the point collocation approach [4, 13, 14], where predictions exhibit a high sensitivity to silencer geometry and also the collocation grid.

ACCEPTED MANUSCRIPT

Temperature variations within a silencer can reach, in some configurations, values around 200ºC [15] and more than 100ºC [16] in the axial and radial directions, respectively. As the temperature distribution can affect the acoustic behavior of the silencer considerably, several authors studied the influence of these gradients in the silencer transmission loss. Kim *et al.* [17] applied an analytic multidimensional approach to some reactive configurations considering axial temperature variation and mean flow. In this work, the silencer was divided into segments of uniform temperature to model the acoustic effect of the thermal gradient, obtaining the acoustic fields in each segment by using the corresponding continuity conditions. Wang *et al.* [18] combined, for a reactive geometry, a segmentation procedure with the boundary element method (BEM) considering uniform mean flow and a linear axial temperature gradient. Sánchez-Orgaz *et al.* [12] considered both axial and radial thermal gradients in a dissipative configuration including an absorbent material and a perforated duct carrying mean flow. As it was shown in this work, the impact of axial thermal variations on the acoustic behavior of dissipative silencers is not as relevant as the radial distribution for the numerical cases under consideration; this is the reason why the current investigation only retains transversal thermal gradients while assuming an axially uniform temperature in both the central duct and the outer chamber, its value being the average temperature of the inlet and outlet sections. A significant reduction in the computational expenditure is then expected if this assumption is suitably combined with the aforementioned point collocation technique. Since the radial temperature gradients can have a considerable influence on the absorbent material properties [12, 19-21], these gradients have been included in the present work by means of an approach allowing the consideration of non-homogeneous properties in the silencer cross section. As the material heterogeneities also have an effect on the acoustic impedance of the perforated surface [22-25], the techniques used in the current context to characterize the silencer performance are numerical in general, due to the complexity of the computations required.

The approach presented by Kirby [4] is here extended to silencers with transversal temperature gradients in the absorbent material and a central perforated passage carrying mean flow. The corresponding thermal-induced material heterogeneities are included in the model through a pressure-based wave equation valid for heterogeneous absorbent materials whose equivalent density and speed of sound depend on the spatial coordinates. A 2D FE approach is applied to the silencer cross section, providing the corresponding acoustic eigenvalues (wavenumbers) and eigenvectors (pressure modes). The complete 3D acoustic field is finally computed combining the transversal solutions of the wave equation

with the point collocation technique to match the pressure and axial acoustic velocity at the expansion/contraction geometrical discontinuities. The results obtained with the proposed mathematical approach are compared with full 3D finite element predictions, showing an excellent agreement while delivering a reduction in the computational effort. The influence of a number of parameters on the acoustic attenuation performance is then investigated, including the effect of the transversal thermal gradient.

2. Mathematical approach

A dissipative silencer with arbitrary (axially-uniform) cross section is shown in Fig. 1. The geometry is divided into four subdomains: the inlet/outlet pipes and a perforated central duct (all carrying mean flow), denoted respectively as Ω_I, Ω_O and Ω_A, and an outer chamber Ω_M with absorbent material. The density and speed of sound in the air ($\Omega_I \cup \Omega_A \cup \Omega_O$) are denoted by ρ_a and c_a, whereas ρ_m and c_m are used for the equivalent acoustic properties [20] of the dissipative region.

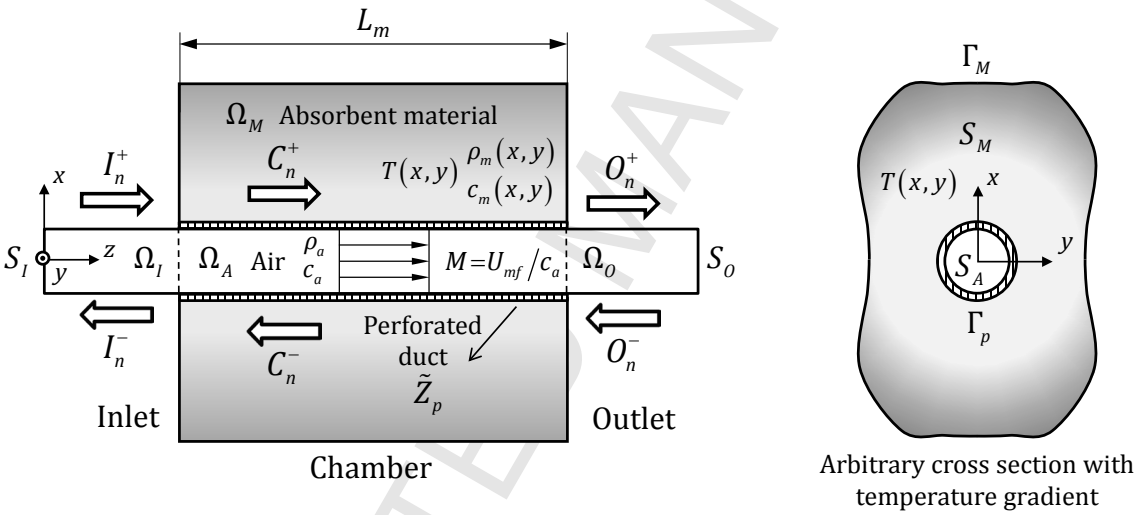

Fig. 1. Perforated dissipative silencer with transversal temperature gradient and mean flow.

As indicated in the Introduction, transversal temperature variations are taken into account over the cross section of the absorbent material S_M. In addition to the silencer geometrical simplification along its length L_m (commonly found in practical applications), axial uniformity is also considered for the variables such as ρ_a, c_a, ρ_m, c_m, the perforated duct impedance $\tilde{Z}_p$ and the mean flow Mach number M, in order to reduce the computational expenditure as much as possible when compared to a three-dimensional finite element analysis. Therefore, any axial temperature gradient is omitted in the

ACCEPTED MANUSCRIPT

mathematical approach, the inlet/outlet temperature average being used to compute the relevant properties and the silencer performance. The validity of this hypothesis is based on earlier models [12] and it will be discussed later with some numerical examples. In the intake and exhaust systems of reciprocating internal combustion engines, the mean flow velocity is small enough for the flow to be assumed as incompressible [1]. This hypothesis is considered in the current investigation.

2.1. Acoustic model of the silencer transversal section

The governing pressure wave equation for the central passage in the presence of a moving medium can be written as [1]

$$\Delta p_a - M^2 \frac{\partial^2 p_a}{\partial z^2} - 2jMk_a \frac{\partial p_a}{\partial z} + k_a^2 p_a = 0 \tag{1}$$

where p_a is the acoustic pressure, k_a is the air wavenumber, defined as $k_a = \omega/c_a$(ω being the angular frequency) and j denotes the imaginary unit.

In the absence of mean flow, the suitable wave equation for a heterogeneous absorbent material can be expressed as [10, 12]

$$\nabla\left(\frac{1}{\rho_m}\nabla p_m\right) + \frac{k_m^2}{\rho_m} p_m = 0 \tag{2}$$

where p_m is the acoustic pressure and $k_m = \omega/c_m$ is the fiber characteristic wavenumber. This equation allows the consideration of the transversal temperature variations within the outer chamber and the corresponding material non-homogeneous properties ρ_m and c_m.

An eigenvalue analysis is carried out from Eqs. (1) and (2) as follows. Since axial uniformity along the z axis is assumed for the material properties and the silencer cross section, the solution of the wave equations is decomposed into axial and transversal functions by using separation of variables. This is also valid for the inlet and outlet ducts, but it is relatively straightforward and the details will be omitted for the sake of brevity. The acoustic pressure in the chamber is therefore expanded in the form

$$p_C(x,y,z) = \Psi(x,y) e^{-jk_z z} \tag{3}$$

where

ACCEPTED MANUSCRIPT

$$\Psi(x,y)=\begin{cases}\Psi^A(x,y), & (x,y)\in S_A\\ \Psi^M(x,y), & (x,y)\in S_M\end{cases} \tag{4}$$

k_z being the axial wavenumber and Ψ^A and Ψ^M the pressure modes associated with the transversal section.

Therefore, the two-dimensional governing equation in the cross section for the central perforated duct can be written as follows

$$\Delta_{xy}\Psi^A+\left(k_a^2-2Mk_ak_z-\left(1-M^2\right)k_z^2\right)\Psi^A=0 \tag{5}$$

where the subscript *xy* represents the 2D transversal coordinate system and Δ_{xy} is the corresponding Laplacian operator. For the outer dissipative chamber, the two-dimensional equation is

$$\nabla_{xy}\left(\frac{1}{\rho_m}\nabla_{xy}\Psi^M\right)+\frac{k_m^2-k_z^2}{\rho_m}\Psi^M=0. \tag{6}$$

2.2. Wavenumbers and pressure modes: transversal eigenvalue problem

Considering first Eq. (5), a FE discretization of the perforated duct cross section is used, together with the Green's theorem and the weighted residuals method [26]. This leads to the following equation for the central duct,

$$-\int_{S_A}\nabla_{xy}\mathbf{N}^T\nabla_{xy}\mathbf{N}\tilde{\boldsymbol{\Psi}}^A\,dS+\left(k_a^2-2Mk_ak_z-\left(1-M^2\right)k_z^2\right)\int_{S_A}\mathbf{N}^T\mathbf{N}\tilde{\boldsymbol{\Psi}}^A\,dS=-\int_{\Gamma_p}\mathbf{N}^T\frac{\partial\Psi^A}{\partial n}d\Gamma \tag{7}$$

where **N** are the usual FE shape functions.

For the outer chamber, the same procedure is applied to Eq. (6), and the governing equation can be written as

$$-\int_{S_M}\frac{1}{\rho_m}\nabla_{xy}\mathbf{N}^T\nabla_{xy}\mathbf{N}\tilde{\boldsymbol{\Psi}}^M\,dS+\int_{S_M}\frac{k_m^2-k_z^2}{\rho_m}\mathbf{N}^T\mathbf{N}\tilde{\boldsymbol{\Psi}}^M\,dS=-\int_{\Gamma_M\cup\Gamma_p}\frac{1}{\rho_m}\mathbf{N}^T\frac{\partial\Psi^M}{\partial n}d\Gamma. \tag{8}$$

Some boundary conditions are required to solve the problem. The outer wall of the chamber is considered rigid and impervious [1], yielding

$$\nabla_{xy}\Psi^M\cdot\mathbf{n}_M=0,\qquad \text{on }\Gamma_M \tag{9}$$

ACCEPTED MANUSCRIPT

$\boldsymbol{n}_M$ being the outward unit normal vector. After applying Eq. (9), the integrals on the right hand side (see Eqs. (7) and (8)) are evaluated over Γ_p only. The acoustic coupling between both subdomains is carried out by means of the perforated duct impedance, considering continuity of the normal acoustic velocity [1, 6]. The kinematic conditions applied over Γ_p are expressed as follows

$$\mathbf{u}_A \cdot \mathbf{n}_A = u_{nA} = -\mathbf{u}_M \cdot \mathbf{n}_M = -u_{nM} = u_n \qquad \text{on } \Gamma_p \tag{10}$$

$$u_n = \frac{\Psi^A - \Psi^M}{\tilde{Z}_p} \tag{11}$$

where Eq. (11) is directly related to the perforated duct acoustic impedance, defined as the ratio of the pressure jump to the acoustic velocity normal to surface. Then, considering the previous equations and the relation between the normal acoustic velocity and normal pressure gradient [1, 6], the following expressions are obtained

$$\frac{\partial \Psi^A}{\partial n} = -\rho_a \left(j\omega u_n - M c_a j k_z u_n \right) = -\rho_a j\omega \left(1 - M c_a \frac{k_z}{\omega} \right) u_n = -\rho_a j\omega \left(1 - M c_a \frac{k_z}{\omega} \right) \frac{\Psi^A - \Psi^M}{\tilde{Z}_p} \tag{12}$$

$$\frac{\partial \Psi^M}{\partial n} = -\rho_m j\omega u_{nM} = \rho_m j\omega u_n = \rho_m j\omega \frac{\Psi^A - \Psi^M}{\tilde{Z}_p}. \tag{13}$$

Now, substituting Eqs. (12) and (13) into Eqs. (7) and (8) yields, respectively

$$\begin{aligned} -\int_{S_A} \nabla_{xy} \mathbf{N}^T \nabla_{xy} \mathbf{N} \tilde{\boldsymbol{\Psi}}^A \, dS + \left(k_a^2 - 2M k_a k_z - \left(1 - M^2\right) k_z^2 \right) \int_{S_A} \mathbf{N}^T \mathbf{N} \tilde{\boldsymbol{\Psi}}^A \, dS \\ = \frac{\rho_a j\omega}{\tilde{Z}_p} \left(1 - M c_a \frac{k_z}{\omega} \right) \int_{\Gamma_p} \mathbf{N}^T \left(\mathbf{N} \tilde{\boldsymbol{\Psi}}^A - \mathbf{N}^* \tilde{\boldsymbol{\Psi}}^M \right) d\Gamma \end{aligned} \tag{14}$$

$$-\int_{S_M} \frac{1}{\rho_m} \nabla_{xy} \mathbf{N}^T \nabla_{xy} \mathbf{N} \tilde{\boldsymbol{\Psi}}^M \, dS + \int_{S_M} \frac{k_m^2 - k_z^2}{\rho_m} \mathbf{N}^T \mathbf{N} \tilde{\boldsymbol{\Psi}}^M \, dS = -\frac{j\omega}{\tilde{Z}_p} \int_{\Gamma_p} \mathbf{N}^T \left(\mathbf{N}^* \tilde{\boldsymbol{\Psi}}^A - \mathbf{N} \tilde{\boldsymbol{\Psi}}^M \right) d\Gamma \tag{15}$$

where the integrals in the right hand side of Eqs. (14) and (15) correspond to the FE load vectors. These involve similar shape functions $\mathbf{N} = \mathbf{N}^*$ for conforming discretizations, while different interpolation functions should be considered for non-conforming meshes [27], $\mathbf{N}^*$ being those associated with region S_M in Eq. (14) and with region S_A in Eq. (15), respectively. Conforming FE are assumed hereafter, thus $\mathbf{N}$ and $\mathbf{N}^*$ being equal.

In compact form, the previous FE integrals can be denoted as

$$\begin{aligned}&\mathbf{K}_A=\int_{S_A}\nabla_{xy}\mathbf{N}^T\nabla_{xy}\mathbf{N}dS,\qquad \mathbf{M}_A=\int_{S_A}\mathbf{N}^T\mathbf{N}dS,\\&\mathbf{F}_{AA}=\int_{\Gamma_p}\mathbf{N}^T\mathbf{N}d\Gamma,\qquad \mathbf{F}_{AM}=\int_{\Gamma_p}\mathbf{N}^T\mathbf{N}^*d\Gamma.\end{aligned}\tag{16-19}$$

Further rearranging gives

$$\mathbf{K}^{AA}=-\mathbf{K}_A+k_a^2\mathbf{M}_A-\frac{\rho_a j\omega}{\tilde{Z}_p}\mathbf{F}_{AA}\tag{20}$$

$$\mathbf{D}^{AA}=-2Mk_a\mathbf{M}_A+\frac{\rho_a jMc_a}{\tilde{Z}_p}\mathbf{F}_{AA}\tag{21}$$

$$\mathbf{M}^{AA}=-\left(1-M^2\right)\mathbf{M}_A\tag{22}$$

$$\mathbf{K}^{AM}=\frac{\rho_a j\omega}{\tilde{Z}_p}\mathbf{F}_{AM}\tag{23}$$

$$\mathbf{D}^{AM}=-\frac{\rho_a jMc_a}{\tilde{Z}_p}\mathbf{F}_{AM}\tag{24}$$

and finally Eq. (14) can be written as

$$\left(\mathbf{K}^{AA}+k_z\mathbf{D}^{AA}+k_z^2\mathbf{M}^{AA}\right)\tilde{\boldsymbol{\Psi}}^A+\left(\mathbf{K}^{AM}+k_z\mathbf{D}^{AM}\right)\tilde{\boldsymbol{\Psi}}^M=\mathbf{0}.\tag{25}$$

Applying the same procedure to the governing equation of the outer chamber, Eq. (15), the following FE matrices are defined

$$\begin{aligned}&\mathbf{K}_M=\int_{S_M}\frac{1}{\rho_m}\nabla_{xy}\mathbf{N}^T\nabla_{xy}\mathbf{N}dS,\qquad \mathbf{M}_{M1}=\int_{S_M}\frac{k_m^2}{\rho_m}\mathbf{N}^T\mathbf{N}dS,\qquad \mathbf{M}_{M2}=\int_{S_M}\frac{1}{\rho_m}\mathbf{N}^T\mathbf{N}dS\\&\mathbf{F}_{MM}=\int_{\Gamma_p}\mathbf{N}^T\mathbf{N}d\Gamma,\qquad \mathbf{F}_{MA}=\int_{\Gamma_p}\mathbf{N}^T\mathbf{N}^*d\Gamma,\end{aligned}\tag{26-29}$$

and introducing the notation

$$\mathbf{K}^{MM}=-\mathbf{K}_M+\mathbf{M}_{M1}-\frac{j\omega}{\tilde{Z}_p}\mathbf{F}_{MM}\tag{30}$$

$$\mathbf{M}^{MM}=-\mathbf{M}_{M2}\tag{31}$$

ACCEPTED MANUSCRIPT

ACCEPTED MANUSCRIPT

$$\mathbf{K}^{MA} = \frac{j\omega}{\tilde{Z}_p}\mathbf{F}_{MA} \tag{32}$$

Eq. (15) can be written in compact form as

$$\left(\mathbf{K}^{MM} + k_z^2\mathbf{M}^{MM}\right)\tilde{\boldsymbol{\Psi}}^{M} + \mathbf{K}^{MA}\tilde{\boldsymbol{\Psi}}^{A} = \mathbf{0}. \tag{33}$$

Thus, the final system of equations obtained from Eqs. (25) and (33) yields

$$\left(\begin{pmatrix}\mathbf{K}^{AA} & \mathbf{K}^{AM}\\ \mathbf{K}^{MA} & \mathbf{K}^{MM}\end{pmatrix} + k_z\begin{pmatrix}\mathbf{D}^{AA} & \mathbf{D}^{AM}\\ \mathbf{0} & \mathbf{0}\end{pmatrix} + k_z^2\begin{pmatrix}\mathbf{M}^{AA} & \mathbf{0}\\ \mathbf{0} & \mathbf{M}^{MM}\end{pmatrix}\right)\begin{Bmatrix}\tilde{\boldsymbol{\Psi}}^{A}\\ \tilde{\boldsymbol{\Psi}}^{M}\end{Bmatrix} = \begin{Bmatrix}\mathbf{0}\\ \mathbf{0}\end{Bmatrix} \tag{34}$$

that can be rewritten in compact matrix form as

$$\left(\mathbf{K} + k_z\mathbf{D} + k_z^2\mathbf{M}\right)\boldsymbol{\Psi} = \mathbf{0} \tag{35}$$

where the following matrices have been defined

$$\mathbf{K} = \begin{pmatrix}\mathbf{K}^{AA} & \mathbf{K}^{AM}\\ \mathbf{K}^{MA} & \mathbf{K}^{MM}\end{pmatrix}, \quad \mathbf{D} = \begin{pmatrix}\mathbf{D}^{AA} & \mathbf{D}^{AM}\\ \mathbf{0} & \mathbf{0}\end{pmatrix}, \quad \mathbf{M} = \begin{pmatrix}\mathbf{M}^{AA} & \mathbf{0}\\ \mathbf{0} & \mathbf{M}^{MM}\end{pmatrix}, \quad \tilde{\boldsymbol{\Psi}} = \begin{Bmatrix}\tilde{\boldsymbol{\Psi}}^{A}\\ \tilde{\boldsymbol{\Psi}}^{M}\end{Bmatrix}. \tag{36}$$

A final eigenvalue problem is obtained from Eq. (35), expressed as

$$\begin{pmatrix}\mathbf{0} & \mathbf{I}\\ -\mathbf{M}^{-1}\mathbf{K} & -\mathbf{M}^{-1}\mathbf{D}\end{pmatrix}\begin{Bmatrix}\tilde{\boldsymbol{\Psi}}\\ k_z\tilde{\boldsymbol{\Psi}}\end{Bmatrix} = k_z\begin{Bmatrix}\tilde{\boldsymbol{\Psi}}\\ k_z\tilde{\boldsymbol{\Psi}}\end{Bmatrix} \tag{37}$$

I being an identity matrix and **0** a matrix containing zeros.

The solution of the eigenproblem defined by Eq. (37) is the basis for the modal expansion presented in section 2.3. For higher order modes, a negative imaginary part of the axial wavenumber k_z is associated with progressive waves while a positive one is associated with regressive waves. Previous to the application of the point collocation technique, the eigenvalues and their associated eigenvectors have to be sorted [4] into an ascending order by the modulus of the imaginary part of the incident waves and by the imaginary part of the reflected waves (an example is provided in Table 1 for the first ten wavenumbers).

Table 1
Eigenvalues associated with the chamber cross section obtained for a mesh with element size 0.01 m: Case A1 (see details in section 3 and also in Table 3), E fiberglass, M=0.1, f=1000 Hz.

Modal number	Progressive wave eigenvalues	Regressive wave eigenvalues
n = 1	14.2133 − 6.8088 j	−16.8420 + 8.4747 j
n = 2	42.1178 − 33.0851 j	−42.0454 + 32.9917 j
n = 3	23.3069 − 59.3160 j	−22.9048 + 59.3167 j
n = 4	12.4230 − 103.6184 j	−12.3971 + 103.2916 j
n = 5	−0.4809 − 141.6255 j	−2.9570 + 143.5955 j
n = 6	9.1813 − 151.1745 j	−7.4097 + 151.7867 j
n = 7	6.2222 − 198.7567 j	−6.1072 + 198.7827 j
n = 8	4.4589 − 248.8107 j	−4.8210 + 248.0599 j
n = 9	0.2814 − 263.7742 j	−1.4565 + 267.1160 j
n = 10	4.1654 − 299.9358 j	−3.9687 + 300.1044 j

2.3. Pressure and velocity fields

Here, the acoustic fields adopt a modal representation [4, 6, 7, 13, 14]. The acoustic pressure in a particular region (inlet/outlet ducts and chamber) can be written in terms of a modal expansion, containing incident as well as the reflected waves. For the inlet duct, the following expression is considered [1, 4]

$$p_I(x,y,z)=\sum_{n=1}^{\infty}\left(I_n^{+}\,\Psi_n^{I+}(x,y)e^{-jk_n^{I+}z}+I_n^{-}\,\Psi_n^{I-}(x,y)e^{-jk_n^{I-}z}\right) \tag{38}$$

while the axial acoustic velocity is given by

$$u_{zI}(x,y,z)=\frac{1}{\rho_a c_a}\sum_{n=1}^{\infty}\left(\frac{k_n^{I+}\,I_n^{+}\,\Psi_n^{I+}(x,y)e^{-jk_n^{I+}z}}{k_a-M\,k_n^{I+}}+\frac{k_n^{I-}\,I_n^{-}\,\Psi_n^{xy-}(x,y)e^{-jk_n^{I-}z}}{k_a-M\,k_n^{I-}}\right) \tag{39}$$

where k_n^{I+}, I_n^{+} and $\Psi_n^{I+}(x,y)$ are, respectively, the axial wavenumber, the pressure modal amplitude and the corresponding pressure mode for the n-th modal term, all of them belonging to the incident wave. Similarly, k_n^{I-}, I_n^{-} and $\Psi_n^{I-}(x,y)$ denote those terms belonging to the

ACCEPTED MANUSCRIPT

reflected waves. The previous definitions can be also used to describe the acoustic fields in the outlet duct, by suitably replacing the modal terms k_n^{I+}, I_n^+ and $\Psi_n^{I+}(x,y)$ by k_n^{O+}, O_n^+ and $\Psi_n^{O+}(x,y)$ (progressive waves) and k_n^{I-}, I_n^- and $\Psi_n^{I-}(x,y)$ by k_n^{O-}, O_n^- and $\Psi_n^{O-}(x,y)$ (regressive waves). It is worth noting that, for ducts with rigid walls, progressive and regressive modes are equal, that is, $\Psi_n^+(x,y) = \Psi_n^-(x,y)$, even in the presence of mean flow [1]. The fundamental mode consists of a plane wave and the associated wavenumber is given by

$$k_1^{I\pm} = \frac{\pm k_a}{1 \pm M}. \tag{40}$$

To compute the acoustic attenuation, the inlet duct is usually assumed to contain an incident plane wave only. Thus, Eqs. (38) and (39) can be rewritten as follows

$$p_I(x,y,z) = I_1^+ \Psi_1^{I+} e^{-jk_1^{I+}z} + \sum_{n=1}^{\infty} I_n^- \Psi_n^{I-}(x,y) e^{-jk_n^{I-}z} \tag{41}$$

$$u_{zI}(x,y,z) = \frac{1}{\rho_a c_a}\left(I_1^+ \Psi_1^{I+} e^{-jk_1^{I+}z} + \sum_{n=1}^{\infty} \frac{k_n^{I-} I_n^- \Psi_n^{I-}(x,y) e^{-jk_n^{I-}z}}{k_a - M k_n^{I-}} \right) \tag{42}$$

where for simplicity $I_1^+ \Psi_1^{I+} = 1$.

The pressure field in the chamber is described by the following expression

$$p_C(x,y,z) = \sum_{n=1}^{\infty}\left(C_n^+ \Psi_n^+(x,y) e^{-jk_{z,n}^+ z} + C_n^- \Psi_n^-(x,y) e^{-jk_{z,n}^- z} \right). \tag{43}$$

Here, it is worth noting that $p_C = p_A$ in Ω_A and $p_C = p_M$ in Ω_M. From Eq. (43), the acoustic velocity field can be expressed as [1, 4]

$$u_{zC}(x,y,z) = \begin{cases} u_{zA}(x,y,z) = \dfrac{1}{\rho_a c_a} \displaystyle\sum_{n=1}^{\infty} \left(\frac{k_{z,n}^+ C_n^+ \Psi_n^{A+}(x,y) e^{-jk_{z,n}^+ z}}{k_a - M k_{z,n}^+} + \frac{k_{z,n}^- C_n^- \Psi_n^{A-}(x,y) e^{-jk_{z,n}^- z}}{k_a - M k_{z,n}^-} \right) & (x,y) \in S_A \\ u_{zM}(x,y,z) = \dfrac{1}{\rho_m c_m} \displaystyle\sum_{n=1}^{\infty} \left(\frac{k_{z,n}^+ C_n^+ \Psi_n^{M+}(x,y) e^{-jk_{z,n}^+ z}}{k_m} + \frac{k_{z,n}^- C_n^- \Psi_n^{M-}(x,y) e^{-jk_{z,n}^- z}}{k_m} \right) & (x,y) \in S_M \end{cases} \tag{44}$$

where again $u_{zC} = u_{zA}$ in Ω_A and $u_{zC} = u_{zM}$ in Ω_M.

2.4. Axial coupling at the geometrical discontinuities. Point collocation.

To obtain the complete description of sound propagation within the silencer, acoustic fields need to be matched at the geometrical discontinuities, that is, the sudden expansion

ACCEPTED MANUSCRIPT

between the inlet duct and the chamber and the sudden contraction between the chamber and outlet pipe. Compatibility conditions are provided by the physical requirements that acoustic pressure and axial velocity be equal at the expansion/contraction and that axial velocity normal to the rigid endplates be zero [1, 4]. Therefore, at the expansion of the silencer the compatibility equations are expressed as

$$p_I(x,y,0)=p_A(x,y,0), \quad (x,y)\in S_I\equiv S_A \tag{45}$$

$$u_{zI}(x,y,0)=u_{zA}(x,y,0), \quad (x,y)\in S_I\equiv S_A \tag{46}$$

$$u_{zM}(x,y,0)=0, \quad (x,y)\in S_M \tag{47}$$

while at the contraction these yield

$$p_A(x,y,L_m)=p_O(x,y,0), \quad (x,y)\in S_O\equiv S_A \tag{48}$$

$$u_{zA}(x,y,L_m)=u_{zO}(x,y,0), \quad (x,y)\in S_O\equiv S_A \tag{49}$$

$$u_{zM}(x,y,L_m)=0, \quad (x,y)\in S_M. \tag{50}$$

If the acoustic pressure and axial velocity in the previous Eqs. (45)-(47) are substituted by their corresponding modal expansions given by Eqs. (41)-(44), the following equations are obtained

$$1+\sum_{n=1}^{\infty} I_n^- \Psi_n^{I-}(x,y)=\sum_{n=1}^{\infty}\left(C_n^+ \Psi_n^{A+}(x,y)+C_n^- \Psi_n^{A-}(x,y)\right) \quad (x,y)\in S_A \tag{51}$$

$$\frac{1}{\rho_a c_a}\left(1+\sum_{n=1}^{\infty}\frac{k_n^{I-} I_n^- \Psi_n^{I-}(x,y)}{k_a-M k_n^{I-}}\right)=\frac{1}{\rho_a c_a}\sum_{n=1}^{\infty}\left(\frac{k_{z,n}^+ C_n^+ \Psi_n^{A+}(x,y)}{k_a-M k_{z,n}^+}+\frac{k_{z,n}^- C_n^- \Psi_n^{A-}(x,y)}{k_a-M k_{z,n}^-}\right) \quad (x,y)\in S_A \tag{52}$$

$$\frac{1}{\rho_m c_m}\sum_{n=1}^{\infty}\left(\frac{k_{z,n}^+ C_n^+ \Psi_n^{M+}(x,y)}{k_m}+\frac{k_{z,n}^- C_n^- \Psi_n^{M-}(x,y)}{k_m}\right)=0 \quad (x,y)\in S_M. \tag{53}$$

Eq. (51) is now enforced pointwise at N_1 collocation points coinciding with the nodes of the FE mesh in section $S_I\equiv S_A$. Similarly, Eqs. (52) and (53) are applied at N_1 and N_2 nodes of the sections S_A and S_M, respectively. In addition, the modal expansions are truncated to a suitable number of terms to guarantee a solvable system of equations. Thus, N_1 equations are obtained for the acoustic pressure field continuity, Eq. (51), that can be written as

ACCEPTED MANUSCRIPT

$$1+\sum_{n=1}^{N_1} I_n^- \tilde{\boldsymbol{\Psi}}_{n,q}^{I-} = \sum_{n=1}^{N_1+N_2} \left(C_n^+ \tilde{\boldsymbol{\Psi}}_{n,q}^{A+} + C_n^- \tilde{\boldsymbol{\Psi}}_{n,q}^{A-} \right) \tag{54}$$

where q = 1, ..., N_1 and $\tilde{\boldsymbol{\Psi}}_{n,q}^{I-}$ and $\tilde{\boldsymbol{\Psi}}_{n,q}^{A\pm}$ refer to the *q-th* nodal value of transversal pressure modes for the inlet pipe and central passage. Similarly, for the axial acoustic velocity continuity over section S_A, the modal summations in Eq. (52) are truncated and enforced at the FE nodes, yielding

$$1+\sum_{n=1}^{N_1} \frac{k_n^{I-} I_n^- \tilde{\boldsymbol{\Psi}}_{n,q}^{I-}}{k_a - M k_n^{I-}} = \sum_{n=1}^{N_1+N_2} \left(\frac{k_{z,n}^+ C_n^+ \tilde{\boldsymbol{\Psi}}_{n,q}^{A+}}{k_a - M k_{z,n}^+} + \frac{k_{z,n}^- C_n^- \tilde{\boldsymbol{\Psi}}_{n,q}^{A-}}{k_a - M k_{z,n}^-} \right). \tag{55}$$

For the rigid wall condition, Eq. (53), the number of collocation points is N_2 and the same number of equations are generated, that is,

$$\sum_{n=1}^{N_1+N_2} \left(k_{z,n}^+ C_n^+ \tilde{\boldsymbol{\Psi}}_{n,q}^{M+} + k_{z,n}^- C_n^- \tilde{\boldsymbol{\Psi}}_{n,q}^{M-} \right) = 0 \tag{56}$$

for q= 1, ..., N_2. As in the previous case, $\tilde{\boldsymbol{\Psi}}_{n,q}^{M\pm}$ refers to the *q-th* nodal value of transversal pressure mode for the absorbent material.

The compatibility equations (48)-(50) at the contraction can be also written in terms of modal expansions. For the computation of the silencer transmission loss, the usual anechoic termination is considered here [1], that is, no outlet reflections are included in the analysis and therefore $O_n^- = 0 \quad \forall n$. Thus,

$$\sum_{n=1}^{\infty} \left(C_n^+ \Psi_n^{A+}(x,y) e^{-jk_{z,n}^+ L_m} + C_n^- \Psi_n^{A-}(x,y) e^{-jk_{z,n}^- L_m} \right) = \sum_{n=1}^{\infty} O_n^+ \Psi_n^{O+}(x,y) \qquad (x,y) \in S_A \tag{57}$$

$$\begin{aligned} &\frac{1}{\rho_a c_a} \sum_{n=1}^{\infty} \left(\frac{k_{z,n}^+ C_n^+ \Psi_n^{A+}(x,y) e^{-jk_{z,n}^+ L_m}}{k_a - M k_{z,n}^+} + \frac{k_{z,n}^- C_n^- \Psi_n^{A-}(x,y) e^{-jk_{z,n}^- L_m}}{k_a - M k_{z,n}^-} \right) \\ &= \frac{1}{\rho_a c_a} \left(\sum_{n=1}^{\infty} \frac{k_n^{O+} O_n^+ \Psi_n^{O+}(x,y)}{k_a - M k_n^{O+}} \right) \qquad (x,y) \in S_A \end{aligned} \tag{58}$$

$$\frac{1}{\rho_m c_m} \sum_{n=1}^{\infty} \left(\frac{k_{z,n}^+ C_n^+ \Psi_n^{M+}(x,y) e^{-jk_{z,n}^+ L_m}}{k_m} + \frac{k_{z,n}^- C_n^- \Psi_n^{M-}(x,y) e^{-jk_{z,n}^- L_m}}{k_m} \right) = 0 \qquad (x,y) \in S_M. \tag{59}$$

Truncating the series with the same criteria as for the expansion, the equations at the collocation points are given by

$$\sum_{n=1}^{N_1+N_2}\left(C_n^{+}\,\tilde{\boldsymbol{\Psi}}_{n,q}^{A+}e^{-jk_{z,n}^{+}L_m}+C_n^{-}\,\tilde{\boldsymbol{\Psi}}_{n,q}^{A-}e^{-jk_{z,n}^{-}L_m}\right)=\sum_{n=1}^{N_1}O_n^{+}\,\tilde{\boldsymbol{\Psi}}_{n,q}^{O+} \tag{60}$$

$$\sum_{n=1}^{N_1+N_2}\left(\frac{k_{z,n}^{+}C_n^{+}\,\tilde{\boldsymbol{\Psi}}_{n,q}^{A+}e^{-jk_{z,n}^{+}L_m}}{k_a-Mk_{z,n}^{+}}+\frac{k_{z,n}^{-}C_n^{-}\,\tilde{\boldsymbol{\Psi}}_{n,q}^{A-}e^{-jk_{z,n}^{-}L_m}}{k_a-Mk_{z,n}^{-}}\right)=\sum_{n=1}^{N_1}\frac{k_n^{O+}O_n^{+}\,\tilde{\boldsymbol{\Psi}}_{n,q}^{O+}}{k_a-Mk_n^{O+}} \tag{61}$$

$$\sum_{n=1}^{N_1+N_2}\left(k_{z,n}^{+}O_n^{+}\,\tilde{\boldsymbol{\Psi}}_{n,q}^{M+}e^{-jk_{z,n}^{+}L_m}+k_{z,n}^{-}O_n^{-}\,\tilde{\boldsymbol{\Psi}}_{n,q}^{M-}e^{-jk_{z,n}^{-}L_m}\right)=0. \tag{62}$$

The algebraic system (54)-(56) and (60)-(62) consists of 4 N_1 + 2 N_2 equations with the same number of unknowns. This is readily solved for each excitation frequency to obtain the unknown pressure amplitudes I_n^{-}, C_n^{+}, C_n^{-} and O_n^{+}.

Finally, the acoustic attenuation can be computed by means of the transmission loss, defined as [1]

$$TL=-20log\left|O_1^{+}\,\Psi_1^{O+}\right| \tag{63}$$

considering that the inlet and outlet ducts are long enough to guarantee the rapid decay of higher order evanescent modes.

3. Temperature-induced property variations

3.1. Absorbent material. Transversal variations of the equivalent acoustic properties

An absorbent material can be defined by its equivalent acoustic properties [20], such as the speed of sound c_m and the density ρ_m (both complex and frequency dependent), or equivalently by its characteristic impedance Z_m and wavenumber k_m. The model employed here is an extension of the empirical power law proposed by Delany and Bazley [28] for rigid fibrous materials, used to calculate c_m and ρ_m in terms of the steady airflow resistivity R. Due to the temperature variations considered in the current investigation, the resistivity is coordinate-dependent over the cross section of the chamber, that is, $R = R(x, y)$. The latter can be calculated at each FE integration point by means of the Christie's power law [19] as follows,

$$R\left(T\left(x,y\right)\right)=R\left(T_0\right)\left(\frac{T\left(x,y\right)+273.15}{T_0+273.15}\right)^{0.6} \tag{64}$$

ACCEPTED MANUSCRIPT

where $R(T_0)$ is the resistivity at the reference temperature T_0 and $T(x, y)$ is the temperature at the integration point. Once the resistivity is computed, the equivalent impedance and wavenumber can be obtained in terms of a number of coefficients a_i, i = 1, 2, ..., 8 derived from a curve fitting process following laboratory measurements, and a dimensionless frequency parameter $\xi = \rho_a f/R$, f being the frequency [20, 28]. For the E fiberglass used in all the computations hereafter, the coefficients are a_1 = 0.220, a_2 = −0.585, a_3 = 0.201, a_4 = −0.583, a_5 = 0.095, a_6 = −0.669, a_7 = 0.169 and a_8 = −0.571, and the reference resistivity is $R(T_0 = 25ºC)$ =30716 rayl/m (for a filling density ρ_b = 120 kg/m^3). The dimensionless frequency parameter calculated as $\xi(x, y) = \rho_a f/R(x, y)$ is also dependent on the coordinates. Thus, the equivalent characteristic impedance Z_m and wavenumber k_m of the absorbent material are also functions of the coordinates and can be obtained by means of the following expressions [10, 20, 28]

$$Z_m(x,y)=Z_a(x,y)\left(1+a_5\xi(x,y)^{a_6}-ja_7\xi(x,y)^{a_8}\right) \tag{65}$$

$$k_m(x,y)=k_a(x,y)\left(1+a_3\xi(x,y)^{a_4}-ja_1\xi(x,y)^{a_2}\right) \tag{66}$$

$Z_a = \rho_a c_a$ and $k_a = \omega/c_a$ being the air characteristic impedance and wavenumber, respectively. All the coefficients a_i are considered constant in spite of the temperature variations, as in previous works [12]. This is consistent with the high temperature results presented by Christie [19] and the recent experimental measurements carried out by Williams *et al.* [21], which have shown the validity of this hypothesis to provide an accurate prediction of the absorbent material properties.

From Eqs. (65) and (66), the equivalent density and speed of sound can be readily obtained as $c_m = \omega/k_m$ and $\rho_m = Z_m/c_m$. These values are introduced in the finite element integrals (26)-(28) to obtain the final eigenvalue problem (37).

3.2. Acoustic impedance of the perforated duct

Several authors have shown the influence of the mean flow and the absorbent material properties on the acoustic impedance of the perforated duct [22-25]. The model of Lee and Ih [23], used in the present work, has been proved to be accurate enough when compared with experimental results. The dimensionless impedance of the perforated screen in the presence of a grazing mean flow can be expressed as

$$\zeta_p=\frac{Z_p}{\rho_a c_a}=\alpha+j\beta \tag{67}$$

ACCEPTED MANUSCRIPT

where the real and the imaginary part of ζ_p can be defined as follows

$$\alpha = \frac{\alpha_0\left(1+\alpha_1\left|f-f_{crit}\right|\right)\left(1+\alpha_2 M\right)\left(1+\alpha_3 d_h\right)\left(1+\alpha_4 t\right)}{\sigma} \tag{68}$$

$$\beta = \frac{\beta_0\left(1+\beta_1 d_h\right)\left(1+\beta_2 t\right)\left(1+\beta_3 M\right)\left(1+\beta_4 f\right)}{\sigma}. \tag{69}$$

It is worth to remark that in Eq. (67) the tilde has been intentionally omitted from the impedance Z_p in comparison with Eq. (11) to indicate that the effect of the absorbent material is not still included on the acoustic behavior of the perforations.

In Eqs. (68) and (69), M is the local mean flow Mach number at the average temperature between the inlet and outlet sections (for further details about the temperature field see section 3.3), d_h the hole diameter, t_p the thickness, σ the porosity and f the frequency. The critical value f_{crit} can be calculated using the expression

$$f_{crit} = \frac{\varphi_1\left(1+\varphi_2 M\right)}{\left(1+\varphi_3 d_h\right)}. \tag{70}$$

The values of the coefficients in Eqs. (68)-(70) were derived from a curve fitting procedure to experimental results [23] and are given in Table 2.

Table 2
Coefficients for the calculation of the acoustic impedance.

Real part (α)	**Imaginary part (β)**	f_{crit}
$\alpha_0 = 3.94\cdot10^{-4}$	$\beta_0 = -6.00\cdot10^{-3}$	$\varphi_1 = 412$
$\alpha_1 = 7.84\cdot10^{-3}$	$\beta_1 = 194$	$\varphi_2 = 104$
$\alpha_2 = 14.9$	$\beta_2 = 432$	$\varphi_3 = 274$
$\alpha_3 = 296$	$\beta_3 = -1.72$	--
$\alpha_4 = -127$	$\beta_4 = -6.62\cdot10^{-3}$	--

The influence of the absorbent material on the acoustic impedance of the perforated duct has to be also included and it can be taken into account by means of the equivalent density of the material [22, 25]. The following expression is used

$$\tilde{Z}_p\left(x_p, y_p\right) = \rho_a c_a\left(\zeta_p + \frac{j0.425 k_a d_h\left(\rho_m\left(x_p, y_p\right)/\rho_a - 1\right)F(\sigma)}{\sigma}\right) \tag{71}$$

ACCEPTED MANUSCRIPT

where x_p, y_p are the transversal coordinates of the particular point where the perforated acoustic impedance is being evaluated. Eq. (71) includes the effects of the mean flow as well as the absorbent material through ζ_p and ρ_m, respectively. Finally, $F(\sigma)$ is related to the acoustic interaction between perforations and it has been obtained by means of the following expression [6]

$$F(\sigma)=1-1.055\sqrt{\sigma}+0.17\left(\sqrt{\sigma}\right)^3+0.035\left(\sqrt{\sigma}\right)^5. \tag{72}$$

3.3. Transversal temperature field

The temperature field in the exhaust system of an automobile depends on many parameters, such as the details of the geometrical configuration, the properties of the different materials composing the exhaust devices, as well as the engine load and speed. In an earlier work [12], it was shown that in spite of the fact that axial temperature gradients can reach values over 100ºC, their influence on the silencer attenuation is relatively low, while transversal gradients can have a great influence on the transmission loss. Therefore, with a view to obtain a numerical approach with a significant reduction in the computational expenditure, the acoustic impact of the axial temperature variation is neglected in the current investigation compared to the transversal one; the temperature along the silencer axis is assumed constant and equal to the average value at the inlet and outlet sections. The transversal gradient in the chamber is retained in the acoustic model due to its considerable influence on the acoustic behavior of the silencer [12]. The numerical test cases presented in the next section approximate the transversal temperature distribution for an axisymmetric configuration by a quadratic polynomial function

$$T_{chamber}(r)=c_0+c_1 r+c_2 r^2 \tag{73}$$

where r is the radial coordinate. Three coefficients are included in Eq. (73) to provide a good agreement with the logarithmic temperature distribution found in cylindrical domain [29]. The quadratic temperature field within the chamber is defined, for example, by prescribing the temperature at three locations: (1) at the perforated screen surface; (2) at the outer radius of the chamber; and (3) at the midpoint between (1) and (2). In this simplified temperature field, no temperature jump has been considered in the perforated surface nor temperature variation has been taken into account inside the perforated central passage, since its dimensions are usually much smaller than those associated with the chamber.

4. Results

The configuration under study consists of an axisymmetric silencer whose dimensions are L_m = 0.3 m, R_1 = 0.0268 m and R_2 = 0.091875 m (see Fig. 2). In addition, the length of the inlet/outlet pipes in the finite element discretizations is L_i = L_o = 0.1 m to guarantee plane wave propagation conditions in the inlet/outlet sections.

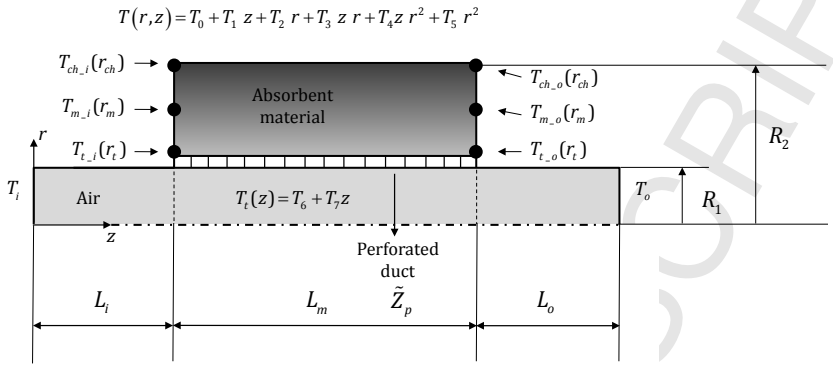

Fig. 2. Silencer with axisymmetric geometry including an axially and radially-varying temperature field.

The temperature fields considered in the computations are shown in Table 3. As can be seen, only radial thermal variations are considered in cases A1, A2 and A3, defined through Eq. (73). These are used for validation of the proposed approach by comparison with full 3D FE computations (see section 4.1. for details). In cases B1, B2 and B3, the temperature field $T(r, z)$ includes both radial and axial temperature gradients, the acoustic impact of the latter and the possible limitations of the current approach being discussed in section 4.2. In addition, some results are presented in section 4.3 regarding the numerical influence of the number of nodes and collocation points associated with the 2D transversal FE mesh.

ACCEPTED MANUSCRIPT

ACCEPTED MANUSCRIPT

Table 3
Temperature distributions.

Case	Inlet temperature	Outlet temperature	Inner radius temperature R_1	Mean radius temperature	Outer radius temperature R_2
	T_i (ºC)	T_o (ºC)	T_{t_i}/T_{t_o} (ºC)	T_{m_i}/T_{m_o} (ºC)	T_{ch_i}/T_{ch_o} (ºC)
A1	250	250	250 / 250	185.48 / 185.48	150 / 150
A2	325	325	325 / 325	228.22 / 228.22	175 / 175
A3	400	400	400 / 400	270.96 / 270.96	200 / 200
B1	300	200	300 / 200	235.48 / 135.48	200 / 100
B2	400	250	400 / 250	303.22 / 153.22	250 / 100
B3	500	300	500 / 300	370.96 / 170.96	300 / 100

4.1. Validation

In order to validate the current numerical approach based on point collocation, several computations have been carried out considering different temperature fields with radial thermal gradient corresponding to cases A1, A2 and A3 (see Table 3). The numerical test problem for each temperature field has been computed twice, including the point collocation technique presented here and a full 3D finite element formulation [12]. For the latter, two possibilities are considered: (1) An in-house code developed in Matlab®, based on a hybrid 3D FE formulation that combines a velocity potential formulation in the central passage and a pressure based-wave equation in the outer chamber [12]; and (2) the FE commercial package COMSOL Multiphysics® software [30]. The in-house FE code allows the consideration of axial and radial temperature gradients, as well as heterogeneous mean flow due to temperature variations, while the commercial package has been only used to validate the point collocation technique when a uniform temperature field of 200ºC is considered in the whole silencer, in the absence of mean flow. From the results shown in Fig. 3, it is evident that good agreement exists in general between the computations provided by the full 3D FE formulation and the point collocation technique, which validates the current approach form a practical point of view. Additionally, it can be also observed that an increase of temperature gradients and mean flow reduces the attenuation of the dissipative silencer, shifting the maximum value of the transmission loss to higher frequencies.

ACCEPTED MANUSCRIPT

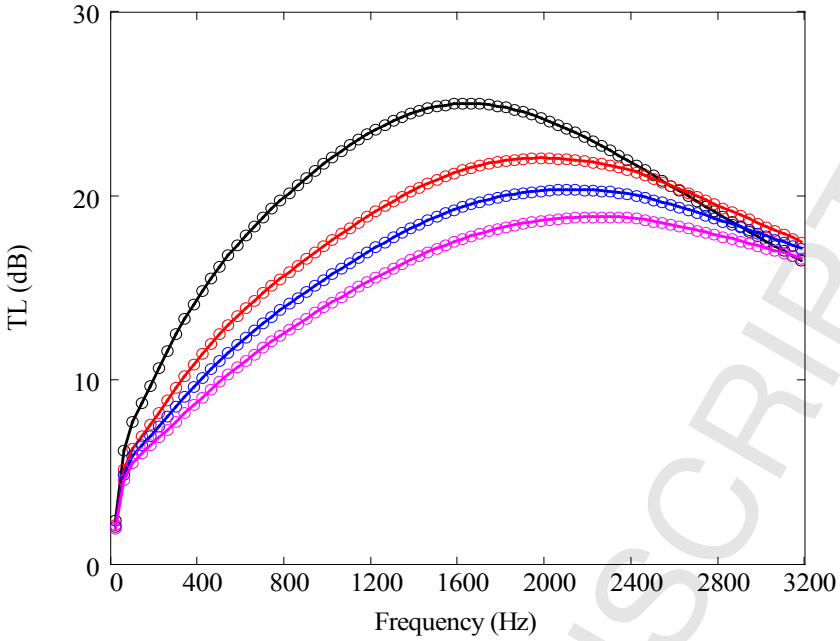

Fig. 3. Transmission loss of a dissipative silencer: —, uniform temperature, M=0, COMSOL; ooo, same, point collocation; —, case A1, M=0.1, in-house code, full 3D FEM; ooo, same, point collocation; —, case A2, M=0.1, in-house code, full 3D FEM; ooo, same, point collocation; —, case A3, M=0.1, in-house code, full 3D FEM; ooo, same, point collocation.

4.2. General temperature fields and TL computations with average values

The application of the point collocation technique requires a uniform temperature along the silencer axis. With a view to assess the impact of this simplification, more general temperature fields are considered in this section including both axial and radial thermal gradients (see cases B1, B2 and B3 in Table 3). The configurations B1, B2 and B3 are calculated using the aforementioned hybrid full 3D FEM formulation [11, 12]. In the outer dissipative chamber, the following quadratic law is taken into account [12, 29]

$$T_{chamber}(r,z)=T_0+T_1 z+T_2 r+T_3 zr+T_4 zr^2+T_5 r^2 \tag{74}$$

where $T_{chamber}$ depends on the radial and axial coordinates. The temperature field is defined from the temperature values depicted in Fig. 2 and detailed in Table 3. In the central pipe, only an axial gradient is considered due to its relatively small dimensions, according to the following expression

$$T_t(z)=T_6+T_7 z \tag{75}$$

where T_6 and T_7 are computed as well by considering the temperature values at the inlet/outlet sections, denoted as T_i and T_o, respectively (see Table 3).

ACCEPTED MANUSCRIPT

The point collocation technique computations of cases A1, A2 and A3 are compared with the full 3D FE transmission loss calculations of configurations B1, B2 and B3. It is worth noting that the radial gradient ΔT_{rad} is given by ΔT_{rad} = 100 °C for A1 and B1, ΔT_{rad} = 150 °C for A2 and B2 and ΔT_{rad} = 200 °C for A3 and B3, respectively. In addition, all the computations have been carried out considering a mean flow Mach number M=0.1.

Two facts can be observed in Fig. 4. First, from a general point of view, as the thermal gradients become higher the attenuation achieved by the silencer is lower. On the other hand, the differences between the transmission loss curves obtained considering both radial and axial thermal gradients simultaneously (cases B1, B2 and B3 computed with the full 3D FE approach), and those considering only radial temperature variations (cases A1, A2 and A3 calculated with the point collocation technique) are stronger as the temperature gradients are higher. For example, the maximum TL discrepancy between the uniform axial temperature field A1 and case B1 is 0.56 dB, while in cases A2 and B2 the discrepancy is about 0.66 dB and in cases A3 and B3 approximately 0.78 dB. However, these values are considered relatively small from a practical point of view, and therefore the slight acoustic impact of replacing the axial temperature gradient by the average value (while retaining the transversal thermal gradient) is clearly compensated by the benefits of a significant reduction of the computational effort if the point collocation technique is used compared to the full 3D FE approach. Further details are provided in section 4.3.

ACCEPTED MANUSCRIPT

ACCEPTED MANUSCRIPT

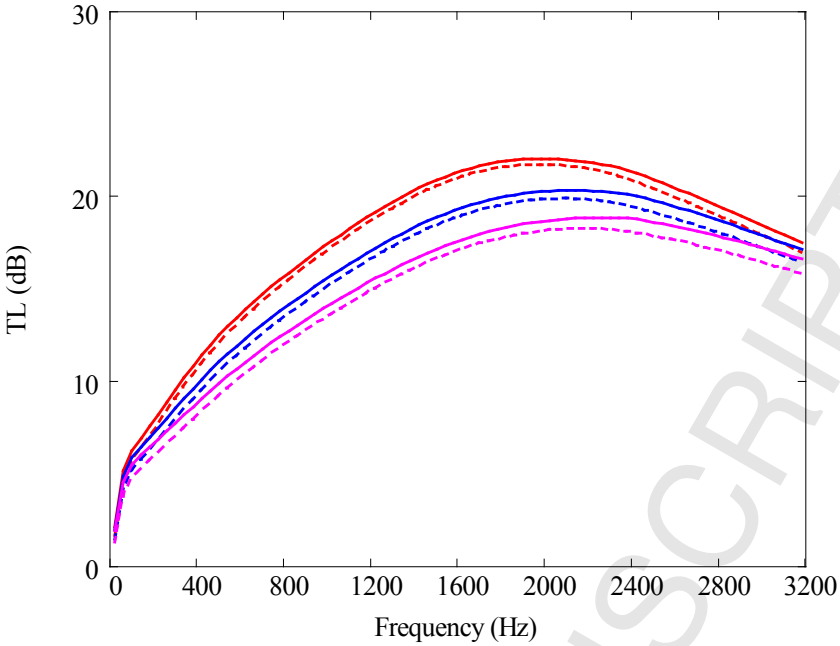

Fig. 4. Transmission loss of a dissipative silencer: —, A1, point collocation; ---, B1, in-house code, full 3D FEM; —, A2, point collocation; ---, B2, in-house code, full 3D FEM; —, A3, point collocation; ---, B3, in-house code, full 3D FEM.

4.3. Numerical influence of the transversal FE mesh

Several computations are carried out in this section with an increasing refinement of the 2D transversal FE mesh associated with the silencer cross section. As the element size is refined, a higher number of nodes is included in the calculations; thus, the accuracy of the solution corresponding to the eigenvalue problem is improved and, additionally, the compatibility conditions of the acoustic fields are enforced at an increasing number of collocation points. As it is shown in this section, this finally leads to a better computation of the silencer transmission loss.

As it was found in earlier studies for silencers with homogeneous materials [4, 7, 13, 14], the number of collocation points and their location have an important effect on the solution accuracy. In the present work, the nodes of the transversal finite element mesh are chosen as collocation points to match the acoustic fields (pressure and axial acoustic velocity). The impact of the element size (and therefore the number of nodes and collocation points) has been studied here by refining the finite element mesh and computing the associated relative error. This can be achieved by comparing the solution of the point collocation technique with a "reference" solution obtained with the full multidimensional FE in-house code previously mentioned in section 4.1. The "reference" transmission loss has been obtained with a FE mesh consisting of 8-node quadratic quadrilateral axisymmetric elements, whose approximate size is 0.002 m. This

ACCEPTED MANUSCRIPT

provides about 50 quadratic elements per wavelength for the maximum frequency f_{max} = 3200 Hz considered in the calculations [31]. The meshes associated with the transversal discretizations of the point collocation technique are composed of 3-node quadratic one-dimensional elements (note that the geometry under analysis is axisymmetric and therefore the silencer cross section is represented by a line), and their corresponding relative error has been computed as follows

$$Error(\%) = \sqrt{\sum_{i=1}^{nfreq}\left(TL_i - TL_i^{ref}\right)^2 \Big/ \sum_{i=1}^{nfreq}\left(TL_i^{ref}\right)^2}\, 100. \tag{76}$$

All the calculations have been executed with frequency increments of 20 Hz in the range from f_{min} = 20 Hz to f_{max} = 3200 Hz, and therefore the number of frequencies is given by *nfreq* = 160 in the summations of Eq. (76). The number of nodes corresponding to each transversal mesh and the approximate element size for the application of the point collocation technique appear in Table 4.

Table 4
Number of nodes of each finite element mesh.

Number of nodes	6	8	14	16	20	22	24	28	30	34	42	50
Element size (m)	0.065	0.032	0.02	0.015	0.0125	0.01	0.009	0.008	0.007	0.006	0.005	0.004

As can be seen in Fig. 5 (in log–log plot), a reduction of the relative error (%) is achieved as the number of nodes in the mesh is increased and the accuracy can be considered satisfactory from a practical point of view. The convergence rate tends to stabilize for meshes having a sufficiently high number of nodes. It can be also noticed that the convergence trend showed by the error is similar for all the temperature gradients considered in the computations.

ACCEPTED MANUSCRIPT

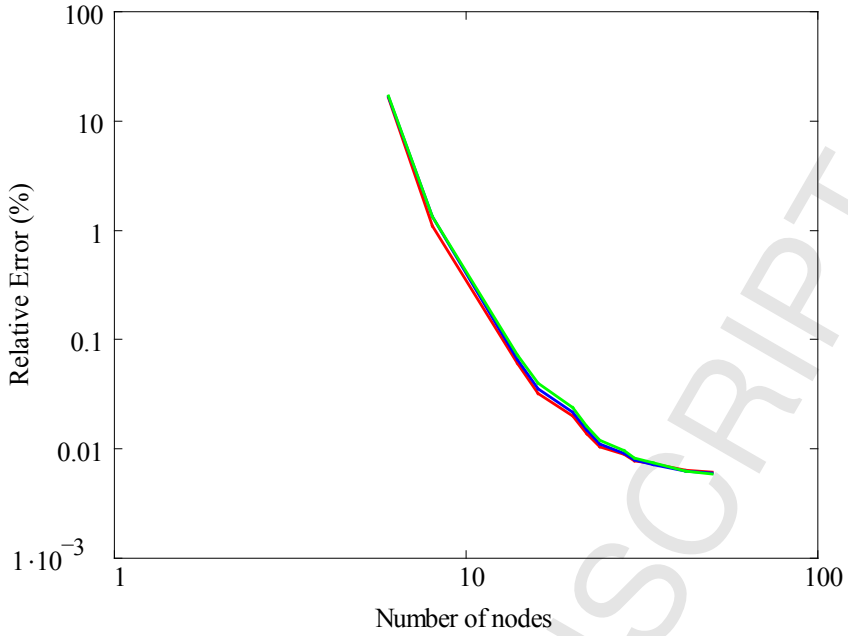

Fig. 5. Relative error (%) between the *TL* obtained with the point collocation technique (with different transversal FE meshes) and the full 3D FEM, mean flow Mach number M=0.1: —, case A1; —, case A2; —, case A3.

The computation expenditure was also obtained for the previous simulations and the results are depicted in Fig. 6. The numerical calculations have been carried out on a Quad-Core, 2.33 GHz machine with 32 GB of RAM and the estimation of the computation time has been generated with the tic toc Matlab® function. The results show that point collocation computation times are below 1 minute in all the cases under study and similar values are obtained for the three temperature gradients considered in the calculations. It is worth noting that the full multidimensional FE formulation requires a considerably higher effort (more than 1 hour per analysis).

ACCEPTED MANUSCRIPT

ACCEPTED MANUSCRIPT

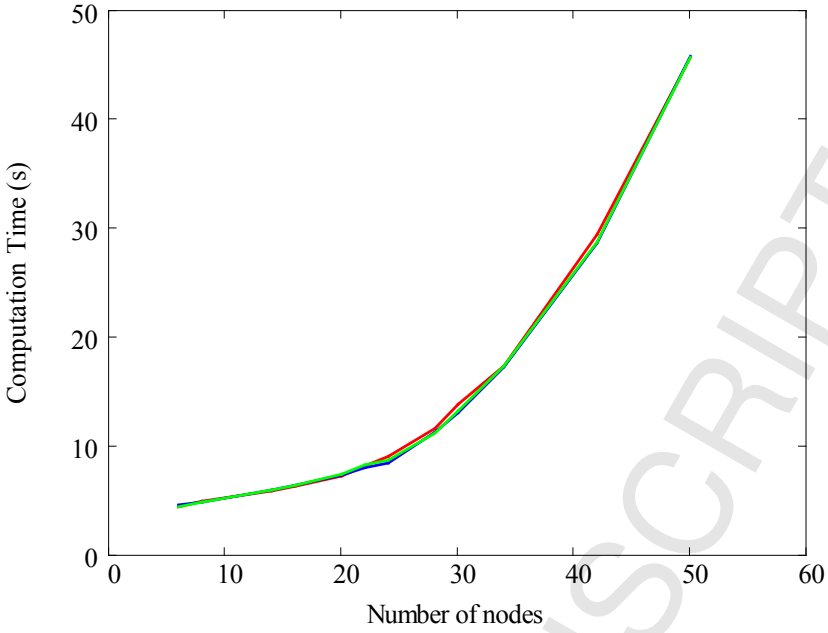

Fig. 6. Computation times of the point collocation technique with different transversal FE meshes, mean flow Mach number M=0.1: —, case A1; —, case A2; —, case A3.

5. Conclusions

A transversal finite element-based eigenvalue problem has been combined with the point collocation technique to model the multidimensional acoustic behavior of perforated dissipative silencers with transversal temperature gradients in the presence of mean flow. The method reduces the computational requirements of a full multidimensional finite element computation in silencers with arbitrary but axially uniform cross section. The proposed acoustic model considers the thermal variations over the silencer cross section, while the axial temperature gradient is replaced by a uniform temperature equal to the average value at the inlet and outlet sections. Thus, the model implemented here is primarily intended for use with silencers for which axial temperature variations have a reduced acoustic impact compared to the transversal thermal gradients. For the perforated central passage, the convective wave equation has been considered to incorporate the influence of the mean flow. Concerning the outer chamber, the absorbent material has been modelled by its complex equivalent acoustic properties. The temperature-induced variations of these properties have been considered through a pressure-based wave equation valid for heterogeneous absorbent materials whose equivalent density and speed of sound depend on the spatial coordinates. The coupling between the perforated central duct and the dissipative outer chamber has been carried out through the corresponding acoustic

ACCEPTED MANUSCRIPT

impedance, whose model has been modified to include the variation of properties with temperature.

First, the aforementioned 2D FE-based eigenvalue problem has been solved for the silencer cross section, providing the corresponding acoustic eigenvalues (wavenumbers) and eigenvectors (pressure modes). Then, the complete 3D acoustic field has been computed combining the transversal solutions of the wave equation with the point collocation technique to match the pressure and axial acoustic velocity at the expansion/contraction geometrical discontinuities. To validate the results obtained using the proposed approach, a comparison has been carried out with full 3D FE computations, showing an excellent agreement. The influence of a number of parameters on the acoustic attenuation performance has been shown, including the effect of the transversal temperature gradient.

6. Acknowledgements

The authors gratefully acknowledge the financial support of Ministerio de Economía y Competitividad and the European Regional Development Fund (project TRA2013-45596-C2-1-R), as well as Generalitat Valenciana (project Prometeo/2012/023).

7. References

[1] M. L. Munjal. Acoustics of Ducts and Mufflers, Wiley, (2014). ISBN 978-1-118-44312-5.

[2] K. S. Peat, K. L. Rathi. A finite element analysis of the convected acoustic wave motion in dissipative silencers, Journal of Sound and Vibration, 184 (1995) 529-545.

[3] W. Wu, Boundary Element Acoustics, WIT Press, (2000). ISBN 1-85312-570-9.

[4] R. Kirby. Transmission loss predictions for dissipative silencers of arbitrary cross section in the presence of mean flow, Journal of the Acoustical Society of America, 114 (2003) 200-209.

[5] R. Barbieri, N. Barbieri. Finite element acoustic simulation based shape optimization of a muffler, Applied Acoustics, 67 (2006) 346-357.

[6] R. Kirby, F. D. Denia. Analytical mode matching for a circular dissipative silencer containing mean flow and a perforated pipe, Journal of The Acoustic Society of America, 122 (2007) 3471-3482.

[7] R. Kirby. A comparison between analytic and numerical methods for modelling automotive dissipative silencers with mean flow. Journal of Sound and Vibration, 325 (2009) 565-582.

[8] F. Piscaglia, A. Montorfano, G. Ferrari, G. Montenegro. High resolution central schemes for multi-dimensional non-linear acoustic simultaion of silencers in internal combustion engines, Mathematical and Computer Modelling, 54 (2011) 1720-1724.

[9] E. Rohan, V. Lukes, Homogeneization of the acoustic transmission through a perforated layer, Journal of Computational an Applied Mathematics, 234 (2010) 1876-1885.

ACCEPTED MANUSCRIPT

[10] A. G. Antebas, F. D. Denia, A. M. Pedrosa, F. J. Fuenmayor. A finite element approach for the acoustic modeling of perforated dissipative mufflers with non-homogeneous properties. Mathematical and Computer Modelling, 57 (2013) 1970-1978.

[11] E. M. Sánchez-Orgaz, F. D. Denia, J. Martínez-Casas, L. Baeza. 3D Acoustic modelling of dissipative silencers with nonhomogeneous properties and mean flow. Advances in Mechanical Engineering, Volume 2014 (2014), Article ID 537935.

[12] E. M. Sánchez-Orgaz, F. D. Denia, J. Martínez-Casas, F. J. Fuenmayor. FE computation of sound attenuation in dissipative silencers with temperature gradients and non-uniform mean flow, 42nd International Congress and Exposition on Noise Control Engineering (Inter-noise), Innsbruck, Austria, (2013).

[13] R. Glav. The point-matching method on dissipative silencers of arbitrary cross-section, Journal of Sound and Vibration, 189 (1996) 123-135.

[14] R. Glav. The transfer matrix for a dissipative silencer of arbitrary cross-section. Journal of Sound and Vibration, 236 (2000) 575-594.

[15] L. J. Ericsson. Silencers, in: D. E. Baxa (Ed.), Noise Control in Internal Combustion Engines, Wiley, (1982) 238-292. ISBN 0-471-05870-X.

[16] X. Hou, X. Guo, Z. Liu, F. Yan, F. Pen. Flow field analysis and improvement of automobile exhaust system cold end, International Conference on Computational Intelligence and Software Engineering, Wuhan, China, (2010).

[17] Y. H. Kim, J. W. Choi, B. D. Lim. Acoustic characteristics of an expansion chamber withs constant mass flow and steady temperature gradient (theory and numerical simulation), Journal of Vibrations and Acoustics, 112 (1990) 460-467.

[18] C. N. Wang, Y. N. Chen, J. Y. Tsai, The application of the boundary element evaluation on a silencer in the presence of a linear temperature gradient, Applied Acoustics, 62 (2001) 707-716.

[19] D. R. A. Christie. Measurement of the acoustic properties of asound absorbing material at high temperatures, Journal of Sound and Vibration, 46 (1976) 347-355.

[20] J. F. Allard, N. Atalla, Propagation of Sound in Porous Media: Modelling of Sound Absorbing Materials, Wiley, (2009). ISBN 978-0-470-74661-5.

[21] P. Williams, R. Kirby, C. Malecki, J. Hill. Measurement of the bulk acoustic properties of fibrous materials at high temperatures, Applied Acoustics, 77 (2014) 29-36.

[22] R. Kirby, A. Cummings. The impedance of perforated plates subjected to grazing gas flow and backed by porous media, Journal of Sound and Vibration, 217 (1998) 619-636.

[23] S. H. Lee, J. G. Ih. Empirical model of the acoustic impedance of a circular orifice in grazing mean flow, Journal of the Acoustical Society of America, 114 (2003) 98-113.

[24] F. P. Mechel. Formulas of Acoustics, Springer, (2008). ISBN 978-3-540-76832-6.

ACCEPTED MANUSCRIPT

[25] I. J. Lee and A. Selamet. Measurement of acoustic impedance of perforations in contact with absorbing material in the presence of mean flow, Noise Control Engineering Journal, 60 (2012) 258-266.

[26] O. C. Zienkiewicz, R. L. Taylor, J. Z. Zhu. The Finite Element Method: Its Basis and Fundamentals, Elsevier Butterworth-Heinemann, (2005). ISBN 978-1-85617-633-0.

[27] F. D. Denia, J. Martínez Casas, L. Baeza, F. J. Fuenmayor. Acoustic modelling of exhaust devices with non-conforming finite element meshes and transfer matrices, Applied Acoustics, 73 (2012) 713-722.

[28] M. E. Delany, E. N. Bazley, Acoustical properties of fibrous absorbent materials, Applied Acoustics 3 (1970) 105-116.

[29] F. P. Incropera, D. P. Dewitt, T. L. Bergman, A. S. Lavine. Principles of Heat and Mass Transfer, Wiley, (2013). ISBN 978-0-470-64615-1.

[30] COMSOL Multiphysics, Acoustic module, Version 4.4, 2014.

[31] F. J. Fuenmayor, F. D. Denia, J. Albelda, E. Giner. H-adaptive refinement strategy for acoustic problems with a set of natural frequencies, Journal of Sound and Vibration, 255 (2002) 457-479.

ACCEPTED MANUSCRIPT